energy&fuels

pubs.acs.org/EF Article

Entrained Flow Gasification of Hardwood Bark: Experimental Characterization of Inorganic Matter versus Equilibrium and Viscosity Predictions

Françoise Defoort,* Boris Grangier, Thierry Chataing, Serge Ravel, Gilles Ratel, and Sylvie Valin

Cite This: *Energy Fuels* 2021, 35, 12151−12164 Read Online

ACCESS | Metrics & More | Article Recommendations | Supporting Information

ABSTRACT: Hardwood bark (HW bark) containing a high ash yield (6.5 wt %) was gasified on a pilot scale in a pressurized entrained flow reactor (EFR, 250 kW_{th}) in allothermal conditions. Conventional physical−chemical characterizations were performed on the ash/slag (ash yield, weight and sieving, inductively coupled plasma, scanning electron microscopy with energy-dispersive spectroscopy, and X-ray diffractometry) and water (pH and ionic chromatography) both collected at the bottom of the EFR. Simulations were performed to predict the phase speciation (solid + liquid + gas) at equilibrium with FactSage 7.3 and its databases and to predict the viscosity with the FactSage "melt" and Thomas models above and below the liquidus temperature, respectively. Results showed that the inorganic matter collected could be characterized with a well closed overall and elemental mass balance. Slight pollution by the alumina wall of the reactor was observed. A very small amount (<4%) of fly ash was noticed. The quench water was acidic as a result of the oxidation of injected N_2 (and not as a result of N biomass). A good consistency was observed between experimental results of the main condensed phases and the prediction either from a simple phase diagram or with global calculations but for only $^1/_4$ of the collected ashes. The remaining ashes, i.e., $^3/_4$, contained unpredicted phases, such as SiO_2 (from soil contaminant) and $CaCO_3$ (from raw HW bark), that did not react together. The viscosity was predicted to be between 1 and 10 Pa s in the 1300−1400 °C temperature range. This viscosity is below the 25 Pa s criteria to have a slag flowing adequately along the EFR wall.

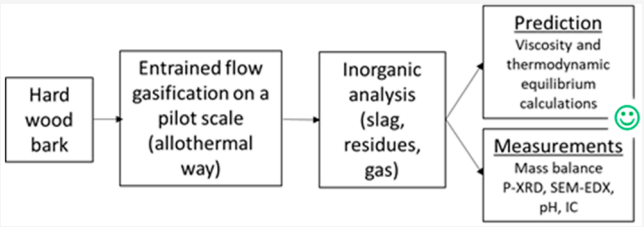

1. INTRODUCTION

The gasification of coal in the entrained flow reactor (EFR) is currently used at industrial scale for heat, power, chemicals, and gaseous or liquid fuels.[1] It is also recognized to be a promising technology for biomass.[2] The main advantages of the EFR over other technologies, such as those using fixed or fluidized beds, are the possible extrapolation to large-scale pressurized plants, the high gas quality (no tars) thanks to its high temperature (>1200 °C), the high carbon conversion of the feedstock into carbon monoxide (and hydrogen), and a good management of the coal ashes. However, the application to biomass is also recognized as not being straightforward as a result of its problematic injection in the EFR and its different ash behavior compared to that of coal.[2] Both the ash-forming elements and the ash yield of biomass are indeed very different from those of coal (Si−Ca−K−Mg−P and 0.1−20 wt % for biomass versus Si−Ca−Al−Fe−Na and 5−50 wt % for coal).[3]

The slagging EFR, in which the ash-forming components melt in the gasifier, then flow down the walls of the reactor, and finally leave the reactor as a liquid slag, is expected to be suitable for biomass as a result of the unavoidable presence of some amount of liquid in its ash.[2,3] There are two types of slagging reactors:[1] one with a hot ceramic insulated wall and another one with a water-cooled membrane wall. In the former, most of the ash deposited on the wall is liquid and wear the ceramic by chemical corrosion (dissolution) and erosion (spalling). The latter is working as a self-crucible thanks to the formation of a protective layer of a solidified slag. The hot wall reactor is more prone to low-ash-yield feedstocks to limit the interaction with the ceramic wall, unlike the water-cooled membrane wall reactor, in which a sufficient amount of ash is necessary to make the self-crucible layer.[1] In both cases, the properties of the liquid ashes (melting temperature and viscosity) are important to avoid clogging the outlet of the gasification chamber, dissolving the ceramic of the hot wall reactor, or disorganizing the protective layer of the solidified slag of the water-cooled membrane wall reactor.

The ash properties and behavior of biomass in slagging EFR gasification are thus important features to be studied and are the purpose of this paper.

Received: April 1, 2021
Revised: June 28, 2021
Published: July 14, 2021

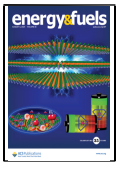

https://doi.org/10.1021/acs.energyfuels.1c00993
Energy Fuels 2021, 35, 12151−12164

Slagging gasification of coal has been studied for a long time on laboratory, pilot, and plant scales. It is known to require a fluxing material, such as limestone, to obtain the adequate properties of the slag at reasonable temperatures.[1] Biomass studies in EFR-like conditions, i.e., fast pyrolysis, are quite numerous on a laboratory scale in a drop tube furnace to study the carbon conversion to syngas, but there are few studies of the ash behavior[4−10] and even less on the pilot scale.[11−15] Autothermal reactors are commonly used on a pilot scale, but no allothermic reactor has ever been studied on a pilot scale for biomass to our knowledge nor at a working pressure of 5 bar. In the former case, a part of the biomass is burned in the O_2 flame to provide heat to the reactor and to ensure the endothermic gasification reaction. In the latter case, external energy is supplied to the reactor. When this external energy is, for example, electrical, it is necessary to add some oxidized agents (H_2O, CO_2, or O_2), otherwise the conditions are pyrolysis. Another solution is to bring external energy by a natural gas/O_2 burner. In this case, the products of the exothermal reaction (from the natural gas burner or fraction of biomass burned) are CO_2 and H_2O that are in a large enough amount to allow for gasification conditions. Allothermic conditions allow for maximization of the conversion of carbon from biomass to synthesis gas (CO and H_2). The purpose of this study is to focus on the slag behavior of biomass on a pilot scale in an allothermal way using a natural gas/O_2 burner at a working pressure of 5 bar.

For instance, some authors have studied, on a laboratory scale, the behavior of the ashes of certain biomasses, such as wood, with a low ash yield[4] and different types of straw[5,6] supported by thermodynamic equilibrium calculations. A small amount of liquid with some solid CaO particles were observed for wood with a low ash yield at temperatures as high as 1450 °C.[4]

Most of the authors using a pilot scale have studied the slag behavior of woody biomass in a hot wall reactor at a medium total pressure (2 bar)[11,13] or higher total pressure (7 bar).[12] Temperatures were from 1050 to 1500 °C. The slags were studied from specific sampling taken along the wall at the bottom colder zone of the reactor (1050−1200 °C) or from slag collected in the quench pool or the reactor outlet. The main finding was the influence of SiO_2−feldspar-rich soil contaminant on woody biomass to generate slag that was otherwise absent or in very low amounts in the same temperature range.[11] Another study performed at a higher pressure (7 bar) at 1200−1320 °C confirmed the effect of adding silica (from a peat resource) to a clean soil-free woody biomass on the flow ability of the slag and the interaction with the aluminosilicate wall.[12] An important finding of the study by Carlsson et al.[13] is the drastic blocking of the reactor outlet when the temperature was increased from 1250−1350 to 1450−1500 °C. However, the initial clean woody biomass had very little ash yield (0.35 wt %) with very low theoretical ash introduced in the reactor (less than 500 g). The reason proposed was a drastic higher content of liquid slag, resulting from the interaction of the aluminosilicate wall with the gaseous KOH species and/or condensed ash. The interpretation by the author was supported by slag characterization, thermodynamic equilibrium, and viscosity calculations.

Very few results were published using biomass on a pilot scale in the configuration of a cold wall reactor. They mostly investigated the thermophysical and chemical properties of real slags collected after testing[14] and studied the slag thickness and deposition rate on the cooled membrane.[15] The feedstocks were slurries derived from low ash yield biomass (<5 wt %), for instance, charcoal from wood and straw pyrolysis, in the bioliq demonstration plant[16]

The objective of this work is therefore to present the behavior of the slag of a hardwood bark (HW bark) biomass containing a high ash yield (6.5 wt % at 815 °C) gasified on a pilot-scale hot wall pressurized EFR (250 kW_{th}). Furthermore, an overall and elemental mass balance of the inorganic matter could be achieved, which is rarely performed in the literature. Conventional physicochemical characterization, scanning electron microscopy with energy-dispersive spectroscopy (SEM−EDS), and powder X-ray diffractometry (P-XRD) of the ash/slag were performed along with thermodynamic equilibrium simulations and viscosity calculations.

This work was performed within the frame of the H2020 Pulp&Fuel project involving 10 partners from 4 European countries. This project received funding from the European Union's Horizon 2020 Research and Innovation Program. It addresses the thermochemical conversion of industrial wastes produced at a pulp and paper mill into biofuel. The project aims at improving gasification performance through dry gasification experiments from dry resources, such as bark (with a fixed-bed reactor and EFR), and supercritical water gasification from wet resources, such as black liquor.

2. MATERIALS AND METHODS

2.1. Feedstock. The HW bark was provided by Fibre Excellence Saint-Gaudens (one of the partners in the Pulp&Fuel project in France). It was chosen because it is a "waste" resource coming from the paper industry and not used in the paper production process. It was ground and sieved with 600 and 300 μm meshes to eliminate large particles and to reduce the fine particle fraction to reach adequate feeding properties for an EFR. A cold injection test with the powder confirmed its ability to be injected in the gasifier. This sieving process caused a significant weight loss of raw material. The mass yield is 30 wt %, which means that 70 wt % of the initial powder could not be used.

The composition after grinding and sieving is shown in Table 1.

Its composition and lower heating value (LHV) is typical of woody biomass, and its ash yield of 6.5 wt % is typical of bark.[3] The main oxides are SiO_2−CaO−K_2O, with SiO_2 being the highest, contrary to woody biomass being usually CaO richer.[3] Furthermore, Al_2O_3 is also quite high for a woody biomass, indicating probable slight soil pollution.

2.2. EFR. The GIROFLE EFR is a hot wall slagging reactor designed to be able to gasify up to 50 kg/h of biomass at 1500 °C, at a total pressure of 30 bar (http://www.cea.fr/cea-tech/liten/genepi/en/Pages/equipements/girofle.aspx). A scheme of the facility is shown in Figure 1.

The reactor is heated with a gas burner (maximum power of 150 kW) fed with natural gas and pure O_2. The external vessel is cooled by cold water flowing into a coiled tube welded onto its outer surface.

The pressure inside the reactor is regulated with valves situated on the exit line. It is measured at different locations of the facility and, in particular, at the top of the reactor.

The biomass is stored in two identical lock hoppers of 100 L each containing up to about 20 kg of fine powder. A dosing screw controls its feeding rate. The biomass is fed at the top of the gasifier. N_2 is injected in the biomass feeding system to avoid hot gas backflow and to assist biomass flow. The solid feeding line ends up at the top of the reactor with a solid injection tube, vertically placed next to the burner and cooled in a double jacket (annular zone cone) by the circulation of neutral gas (N_2 optionally mixed with helium or argon), even when biomass has not yet been injected.

An alumina tube of 0.25 m in diameter and 0.014 m in thickness delimits the internal part of the reactor. Refractory bricks (0.23 m

https://doi.org/10.1021/acs.energyfuels.1c00993
Energy Fuels 2021, 35, 12151−12164

Table 1. Composition and Characteristics of the Feedstock Introduced

	HW bark
moisture (wt %, ar[a])	9.0
LHV[a] (MJ/kg)	17.8
ash at 815 °C (wt %, db[a])	6.5
C (wt %, db[a])	49.2
H (wt %, db[a])	5.63
N (wt %, db[a])	0.35
S (wt %, db[a])	0.03
Cl (wt %, db[a])	0.025
O (by difference) (wt %, db[a])	37
Al (mg/kg, db[a])	1690
Ca (mg/kg, db[a])	15174
Fe (mg/kg, db[a])	976
Mg (mg/kg, db[a])	866
Mn (mg/kg, db[a])	238
P (mg/kg, db[a])	329
K (mg/kg, db[a])	2728
Si (mg/kg, db[a])	12476
Na (mg/kg, db[a])	316
Ti (mg/kg, db[a])	76
Pb (mg/kg, db[a])	2
Zn (mg/kg, db[a])	60
SiO_2 (wt % ash calculated)	45.7
CaO (wt % ash calculated)	36.4
Al_2O_3 (wt % ash calculated)	5.5
K_2O (wt % ash calculated)	5.6
Na_2O (wt % ash calculated)	0.7
MgO (wt % ash calculated)	2.5
Fe_2O_3 (wt % ash calculated)	2.4
P_2O_5 (wt % ash calculated)	1.3

[a]LHV, lower heating value; db, dry biomass; and ar, as received.

thick) made of Al_2O_3 and SiO_2 surround this tube. These bricks ensure the thermal insulation. The internal part of the reactor is divided into two parts. The upper part (about 1 m long) is heated by the burner and constitutes the reactive zone. The lower part is the quench zone, which can be cooled by either deionized water or N_2, in both cases with three nozzles located at the same level.

The height between the top of the quench zone and the lateral exit of the gas is about 1.25 m. The gas then flows into a heat exchanger, in which water is condensed, and through filters before being burnt in a post-combustion unit.

The bottom of the reactor is filled with deionized water, whose level is regulated all along the experiment. Slags made of biomass ash are solidified when falling in this water.

Thermocouples are positioned at 11 levels in the reactor. For each level, several thermocouples are distributed radially from the cooled vessel to the internal alumina wall. For the analysis of experimental results, we are going to consider the measurements of the thermocouples situated near the internal wall of the reactor because their values are the closest to the gas and biomass temperature.

A constant N_2 flow rate is introduced in the reactor as a protection gas for the windows and in an annular space outside the internal reactor.

The total dry gas flow rate is measured after the heat exchanger with a Coriolis mass flowmeter. Moreover, helium as a tracer gas is introduced with a controlled flow rate on the exit line before the heat exchanger.

Gas composition is analyzed by a micro gas chromatograph (μGC), which allows for quantification of the volume content of the gas species coming from gasification (H_2, CO, CO_2, CH_4, C_2H_4, C_2H_6, C_2H_2, C_3H_8, C_6H_6, C_7H_8, H_2S, COS, etc.) and the injected gas species (O_2, He, and N_2). One analysis is performed every 3 min.

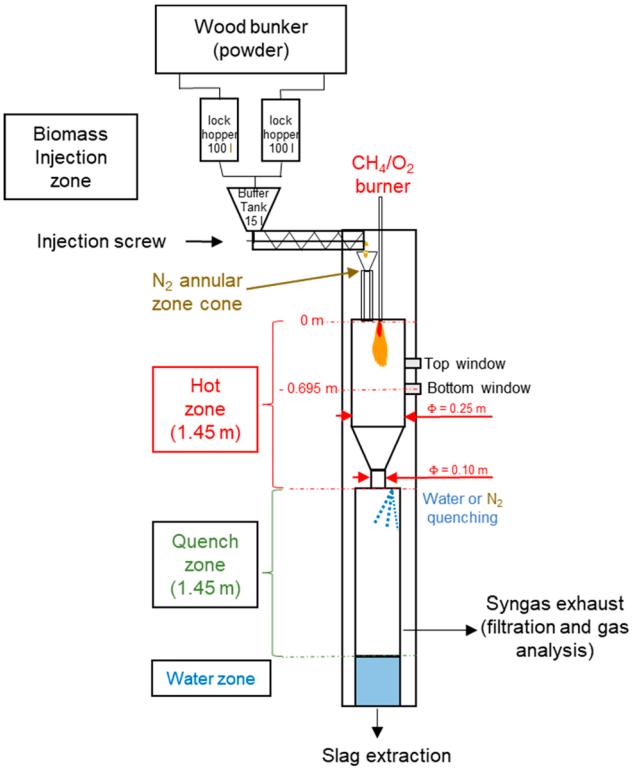

Figure 1. Scheme of the EFR facility.

2.3. Experimental Procedure. The days before the experiment, the reactor is first preheated up to more than 700 °C thanks to natural gas combustion in the burner, with a reactor pressure of 2 bar. Then, the pressure in the reactor is very progressively increased up to the target value, keeping the same combustion power.

On the day of the experiment, the burner power is adjusted to reach the target temperature of the test. When biomass starts to be fed, the burner power is first increased and then stabilized to keep the target temperature in the reactor.

2.4. Characterization of Residues. After the test, the bottom of the reactor was opened to recover the water and solid residues. The collected residues were dried, weighted, and sieved with several mesh sizes (100, 630, and 2500 μm). The first two approximately corresponded to the initial biomass particle size.

Several analyses were performed in each class of residue: weighing, measurement of the ash yield at 815 °C (the complement to this ash yield is estimated to be unburned carbon), chemical composition measured by inductively coupled plasma (ICP) spectrometry, and presence of amorphous and crystalline phases analyzed by powder X-ray diffraction (P-XRD). A D8 Bruker Advance apparatus with Cu Kα radiation (40 kV and 30 mA) equipped with a fast Lynxeye detector was used. The samples were ground to the consistency of a fine flour if necessary. Approximately 0.5 g of ash was placed in an amorphous silica sample holder and flattened with a microscopy glass. Diffractograms were obtained over a 2θ interval between 10° and 70°. Phase analysis was performed with DIFFRAC Plus/EVA software using the International Centre for Diffraction Data (ICDD) database PDF-4.

Some slag samples were analyzed by scanning electron microscopy (SEM) coupled with energy-dispersive X-ray spectroscopy (EDS) for morphology and elemental composition (semi-quantitative) of the observed phases. The instrument used was a Philips XL30 SEM coupled with an Oxford Instruments EDX system (INCA software). The slags were embedded under vacuum in epoxy resin and polished with water-free lubricants. The samples were coated with graphite to make them conductive, allowing for SEM analysis.

https://doi.org/10.1021/acs.energyfuels.1c00993
Energy Fuels 2021, 35, 12151−12164

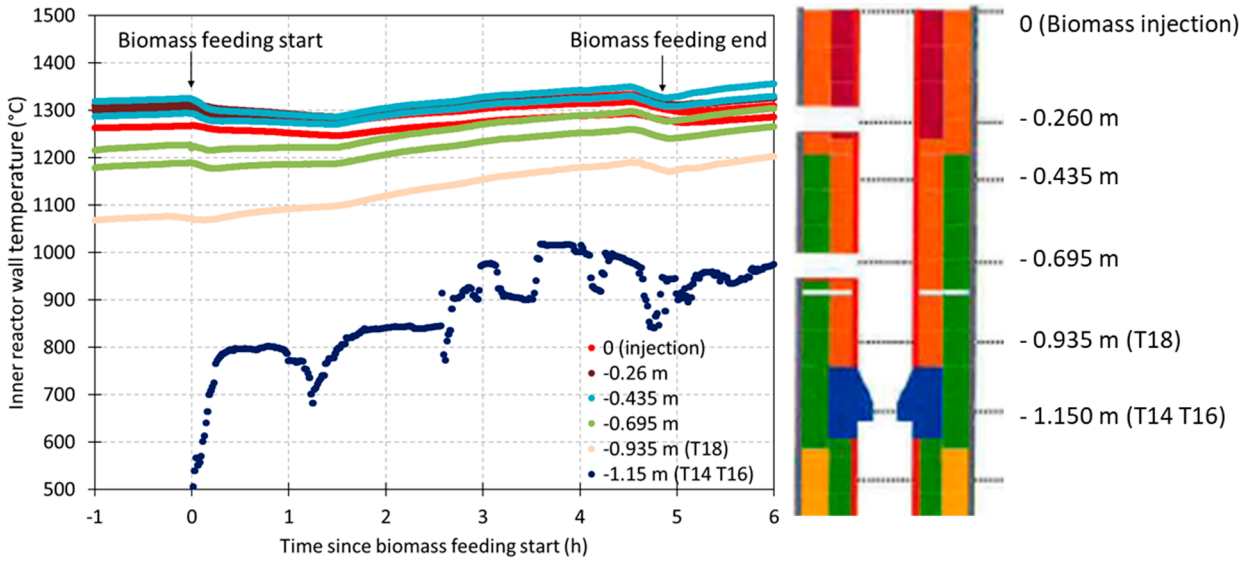

Figure 2. Temperatures measured as a function of time and position of the thermocouples along the upper part of the reactor.

The water collected at the bottom of the EFR was weighed and analyzed by pH-metry and ionic chromatography (IC) to obtain anions and cations.

2.5. Simulation Tools. *2.5.1. Thermodynamic Calculations.* The thermodynamic calculations were performed by minimization of the Gibbs free energy of the total system with the FactSage software 7.3 and adequate databases.[17] The compound database FactPS for the gas phase and FToxid database for the oxide solid and liquid solution phases were used. They are used to predict all phases (solid + liquid + gas) at equilibrium at any temperature and any total pressure. The software allows for all solid and liquid solutions in the calculations to be taken into account. For some of them, the user has to choose. The complete list of these solutions is reported in Table S1 of the Supporting Information. The main solutions found at equilibrium are the liquid solution (SLAGA) and the solid solutions (KASH, WOLLA, LEU1, OlivA, Mel, and Feld).

The condensed phases at equilibrium were calculated first using a simplified method consisting of a ternary phase diagram with the three main oxides of the feedstock ashes (SiO_2−CaO−K_2O) and second using the "equilib" module referred to as global calculations, taking into account the atmosphere, the total pressure, and all of the elements of the feedstock. This allowed for the inorganic volatilities to be taken into account and simulation of the inorganic fractionation between the gas and condensed phases. The initial inputs were the quantities of gas from the burner (O_2 and CH_4) and those of the neutral gas introduced (N_2) per kilogram per hour of HW bark introduced (Tables S2−S4 of the Supporting Information). The total pressure was 5 bar, and the temperature was varied between 800 and 2000 °C. The results of the condensed phases were plotted in grams per kilogram of dry biomass. The volatilization of each element was plotted in grams per introduced gram (or moles per introduced mole).

Some calculations were also performed taking into account the ceramic refractory wall material interaction with the ashes, i.e., dense alumina in the upper part and refractory concrete (60% Al_2O_3−40% SiO_2) in the lower conical part. The temperature of 1150 °C was chosen because it is close to that measured in the lower part of the refractories next to the cone (Figure 2). The input data were the same mass balance (1 kg of biomass + atmosphere) as previously but adding a small amount of each kind of refractory. A maximal mass of 20 g was chosen because it corresponds to an ablated refractory crown estimated about 0.001 m in depth and 0.02 m high in the conical part of the reactor (3.14 × 0.1 × 0.02 × 0.001 × 3.2 with refractory density = 3.2 g/10^{-6} m^3).

2.5.2. Viscosity Calculations. Viscosity of the liquid slags can be predicted thanks to simple models (like from Seiler[18] with the Urbain model[19]) or more sophisticated models taking into account the structure of the liquid phase.[20−22]

In this report, we calculated the viscosity of the slag using the FactSage model "melt".[20]

Below the liquidus temperature, a solid fraction is appearing and drastically increases the viscosity. The model of Thomas[23] was used to calculate the apparent viscosity of this semi-solid mixture. This model was established for hydrodynamic suspensions; thus, there is no certainty about their relevance in the case of ash. Other models exist;[24] however, they involve parameters whose physical meaning is not always well-defined or which are not known in the case of suspensions formed by a mixture in the course of solidification.

The semi-solid viscosity $\eta_{semi\text{-}solid}$ is therefore calculated using the Thomas formula (eq 1)

$$\eta_{semi\text{-}solid} = \eta_{liq}[1 + 2.5f_{vs} + 10.05f_{vs}^{2} + 0.00273\exp(16.6f_{vs})] \quad (1)$$

where η_{liq} is the viscosity of the liquid phase in equilibrium and f_{vs} is the solid volume fraction.

The solid volume fraction f_{vs} is calculated from the volumes occupied by each phase v_{solid} and v_{liquid} (eq 2)

$$f_{vs} = (\sum v_{solid})/(\sum v_{solid} + \sum v_{liquid}) \quad (2)$$

with

$$v_{solid} = m_{solid}/d_{solid}$$

$$v_{liquid} = m_{liquid}/d_{liquid}$$

The volume of the phases v_{solid} and v_{liquid} were calculated from their density and from the mass calculated by FactSage (m_{solid} and m_{liquid} = m_{SLAGA}).

The density of the liquid phase d_{liquid} is estimated by the additivity rule of molar mass and molar volume of the oxides constituting the liquid phase (in molar fraction) (eq 3)

$$d_{liquid} = (\sum_{iox} X_{iox}M_{iox})/[(1 + 0.0001(T_{slag} - 1773))(\sum_{iox} X_{iox}V_{iox})] \quad (3)$$

where iox is the oxides of the liquid phase (SiO_2, CaO, etc), M_{iox} is the molar mass of oxide, and V_{iox} is the molar volume of oxide in its liquid state at 1773 K (Table 2). The temperature coefficient (dV/dT) is assumed to be 0.01%/K for each one.[25] X_{iox} is the molar fraction of oxide of the liquid-phase SLAGA. This quantity is not

https://doi.org/10.1021/acs.energyfuels.1c00993
Energy Fuels 2021, 35, 12151−12164

Table 2. Molar Mass and Liquid Molar Volume at 1773 K of Oxides with Their References

iox	M_{iox} (g/mol)	V_{iox} at 1773 K ($\times 10^{-6}$, m^3/mol)
Fe_2O_3	159.68	38.4[25]
FeO	71.84	15.8[25]
CaO	56	20.7[25]
K_2O	94.2	47.28[26]
SiO_2	60.08	26.86[26]
Al_2O_3	101.96	37.42[26]
MgO	40.3	16.1[25]
Na_2O	62	33[25]

given by the software and must be calculated, for example, from the elemental molar composition of SLAGA (Mol-i_FToxid-SLAGA).

The density of the solid phases d_{solid} are reported in Table 3. Several solid phases are calculated to be in equilibrium with the liquid phase. Only the main ones were taken into account. No effect of thermal expansion was taken into account.

Table 3. Density of the Solid Phase (FactSage)

	d_{solid} (g/10^{-6} m^3)
WOLLA ($CaSiO_3$)	2.90
$Ca_3MgSi_2O_8$	3.34
OlivA $(Ca,Mg,Fe)_2SiO_4$)	3.3
KASH ($KAlSiO_4$)−LEU1 ($KAlSi_2O_6$)	2.5

3. RESULTS AND DISCUSSION

3.1. Progress of the Test, Process Temperatures, and Syngas. Conditions of the tests are shown in Table 4. The injection of HW bark powder was stable for 5 h with a powder flow rate of 6 kg/h corresponding to 30 kg injected, a total pressure of 5 bar, and a burner power of 33 kW to be in an allothermal mode. The oxidant (O_2) brought into the system comes from the natural gas burner and straightly reacts with the natural gas. The equivalent ratio associated with natural gas (ER_nat-gas) is 1.0. However, a global equivalent ratio (ER_global) considering all combustible species (natural gas and biomass) can also be calculated (ER_global = 0.55).

Table 4. Stabilized Conditions of the Test

	test conditions
test duration	4 h and 42 min
biomass flow rate (kg/h)	6.13
total input mass (kg, ar[a])	30.355
total pressure (bar)	5
burner power (kW)	33
natural gas (CH_4) (Nm^3/h)	3.4
O_2 (Nm^3/h)	6.8
N_2 (Nm^3/h)	7.53
water quench (L/h)	6.5
mean wall temperature between 0 and −0.435 m (°C)	1280−1330

[a]ar = as received.

The water quench was injected as a water spray at the reactive zone exit to cool gases and ashes.

The temperatures (Figure 2), gas analyses, and combustion power of the burner (Figure 3) measured show that the gasification was stable all along the test. No blockage linked to the ash management was observed during the test, even if about 1.8 kg of theoretical ash was injected.

The temperatures measured at different heights are rather uniform along the reactor wall from the biomass injection zone down to 0.435 m from the injection level. At 0.695 m from the injection, the temperature starts to be lower. The maximum temperature is around 1300−1350 °C during biomass feeding. The power of the burner is increased from about 22 to 33 kW when biomass starts to be fed into the gasifier, to keep a constant temperature. However, the power is decreased at the end of the biomass injection period even if the temperature still increases as a result of the progressive decrease of the biomass feeding rate approaching the emptying of the lock hoppers.

The maximum temperature measured in the cone level at 1.15 m from the injection level (T14−T16) is around 1000 and 1200 °C at the level above (T18 of 0.935 m). The refractory along the reactor is dense Al_2O_3 in the upper part and a concrete Al_2O_3−SiO_2 refractory in the conical part (at 1.15 m from the injection level).

As expected, the main gaseous species during the biomass injection are H_2, CO, H_2O (not measured), and CO_2. These are produced from the biomass thermochemical conversion and are mixed or react with CO_2 and H_2O coming from the natural gas combustion. The H_2/CO molar ratio is close to unity (0.9).

The CH_4 content is comprised between about 0.5 and 1.5 vol % and is followed by C_2H_4, with a content 10 times smaller than that of CH_4, following the same variations. All of the other gaseous species have a concentration under 0.05 vol %.

These results obtained in an allothermal EFR using a natural gas/O_2 burner are in agreement with the literature[11−13] for such a temperature range and biomass feedstocks obtained in an autothermal EFR.

3.2. Residues and Liquid Characterizations. About 1.9 kg of dried residue (dry basis) was collected at the bottom of the EFR (Figure 4). Only a few grams of residues were collected on the filters at the exhaust of the EFR. Some traces were also observed on the windows at the top of the reactor.

3.2.1. Residues Collected on the Windows. The residues collected on the windows were analyzed by SEM on graphite rubber (Figure 5).

The white residues observed on the top window are composed of spheres of about 10 μm in diameter, which are very rich in CaSiAlK and look like silicate liquid droplets.

On the contrary, the black residues observed on the bottom window are mainly composed of unburned carbon or soot.

3.2.2. Residues Collected in the Filter at the Exhaust of the Reactor. The residues collected on the filter were analyzed by SEM on graphite rubber (Figure 6).

They mainly constitute carbon with some rare tiny glassy spheres (solidified slag).

3.2.3. Residues Collected at the Bottom of the Reactor. The residues collected at the bottom of the reactor were dried, weighed (1887 g), and sieved in different classes (Table 5).

The particle size of the residue in the class of 100−630 μm has the higher mass fraction (61 wt %) and mainly corresponds to the initial particle size of the biomass. Only 23 wt % of the residues look like slag, mostly green ($^2/_3$) or black ($^1/_3$) (Figure 7).

The ash yield at 815 °C was measured for each class of residue, except the class of >2500 μm (Table 5). It is between 42 and 57 wt %, indicating that some ungasified carbon (650 g) was still present, corresponding to 4.8% of introduced

https://doi.org/10.1021/acs.energyfuels.1c00993
Energy Fuels 2021, 35, 12151−12164

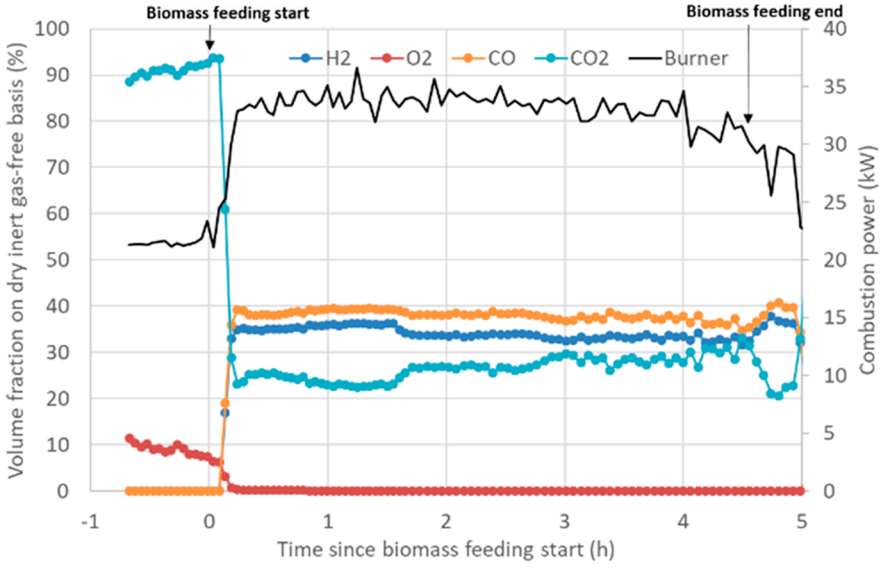

Figure 3. Dry inert gas-free gas composition as a function of time (major species) and combustion power of the burner.

Figure 4. Residues collected at the bottom of the EFR, exhaust, and on windows.

carbon. This means that more than 95% of introduced carbon has been gasified, which is very good.

The chemical composition of raw HW bark (turquoise) and each class of collected residues (orange and yellow) as well as the black and green slags (black and green, respectively) are presented in Figure 8.

A clear increase of the alumina contents is observed for all of the residues collected compared to the raw HW bark (in turquoise). The smaller class of slag (<100 μm, in yellow) is richer in CaO. The other classes are depleted in CaO (except the black slag) and K_2O.

The green slag was characterized by P-XRD and SEM−EDS (panels a and b of Figure 9). The black slag and the residues of <100 and 100−630 μm were characterized by P-XRD only (Figure 9c).

An amorphous matrix (silicate liquid) with $CaSiO_3$ (wollastonite) and SiO_2 (quartz), crystalline phases, is present in the green slag (panels a and b of Figure 9). A good agreement is observed between P-XRD and SEM−EDS. The amorphous phase composition is close to the global ICP measurements (slightly depleted in Si and Ca as a result of $CaSiO_3$ and SiO_2). Pollution by alumina (probably coming from the reactor wall) is also observed. The large SiO_2 phase observed by SEM in the green slag sample seems to indicate some remaining silica pollution that may not be in equilibrium with the whole rest of the slag.

The black slag contains almost no amorphous phase (no liquid) and is much more crystallized with $CaSiO_3$ but also contains a lot of aluminosilicate crystalline phase doped with Ca, Fe, and Mg (gehenite akermanite) (Figure 9c). It seems to have solidified more slowly than the green slag, allowing all phases to have time to crystallize, which may explain its black rather than green color. It could have stayed on the conical wall of the reactor before falling into the water. These green/black-colored slags were also observed by Carlsson et al.[13] with the same amorphous/crystallization P-XRD observations and higher alumina contamination of the black-colored slag. The authors also deduced a different solidification path.

The amorphous phase (bump) and $CaSiO_3$ (wollastonite) that were observed in the green slag are not observed in the smaller particle fraction (<100 and 100−630 μm) in Figure 10. For both fractions, the same crystalline phases SiO_2 (quartz) and $CaCO_3$ (calcite) are observed.

It is surprising to find $CaCO_3$. Indeed, if we reasonably assume that it is naturally present with CaC_2O_4 (calcium oxalate) in a raw woody biomass,[3,27] the high temperatures encountered in the reactor (>1300 °C) should have made it react with the other oxides of the feedstock (silicate and/or alkalis) or, if in excess, should have decomposed it into CaO and CO_2 (g). However, CaO is not stable and, when cooled, will spontaneously, for one part, react to the high CO_2 (g) concentration in the syngas (several volume percent) and be converted to calcium carbonate $CaCO_3$ and, for the other part, react with the water from syngas or quench and be converted to calcium hydroxide $Ca(OH)_2$. These calcium oxides, when falling in the acidic water at the bottom of the reactor, are probably partly dissolved (see section 3.2.4), and only calcium carbonate remains when the residue is collected and dried. Another explanation would be that the residence time in the hot zone of the reactor is too short for its decomposition/reaction with silicate and/or alkalis to have time to take place.

3.2.4. Water Collected at the Bottom of the Reactor. The water collected at the bottom of the reactor was analyzed

https://doi.org/10.1021/acs.energyfuels.1c00993
Energy Fuels 2021, 35, 12151−12164

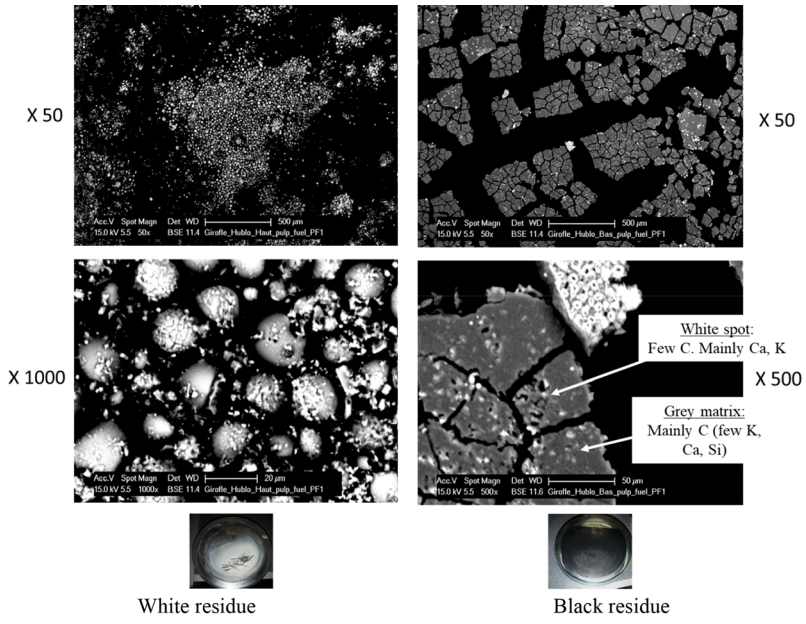

Figure 5. Scanning electron microscopy with backscattered electrons (SEM−BSE) on residues collected on windows (EDX shown in Table S5 of the Supporting Information).

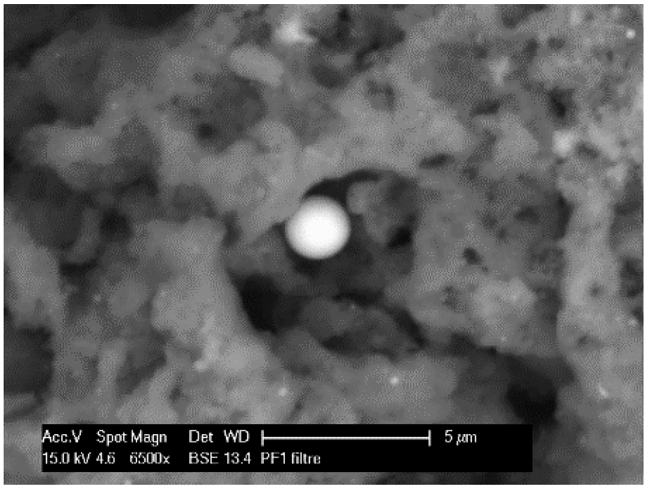

Figure 6. SEM−BSE of residues collected in the filter.

Table 5. Mass Fraction and Ash Yield (815 °C) in the Different Particle Size Classes

residues (bottom EFR) (μm)	mass fraction (wt %)	ash yield at 815 °C (wt %)
>2500	23	100[a]
630−2500	9	42
100−630	61	57
<100	7	57

[a]Not measured.

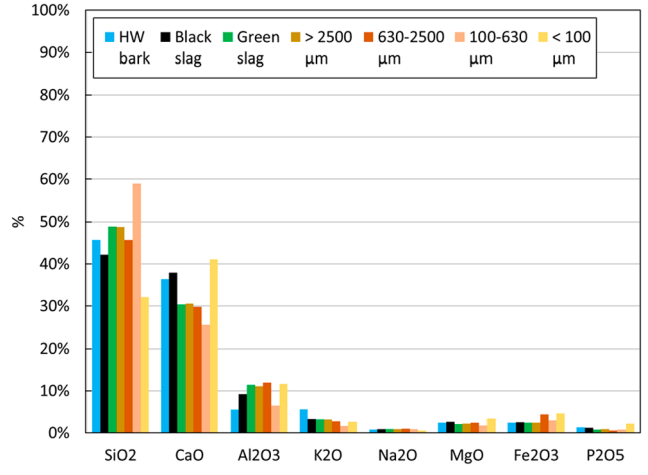

Figure 8. Chemical composition of raw HW bark and collected residues in ash weight percent.

(Table 6). The total mass of water representative of the sampling was estimated to be 500 L. This volume takes into account the maximum mass (volume) of water that remains in the reactor all along the test (450 L) and the water coming from the burner during the biomass injection, from biomass gasification and from the water quench (~50 L). The water produced during the heating of the reactor before the biomass injection (~200 L) is not taken into account because this water overflows outside the reactor. The inorganic elements

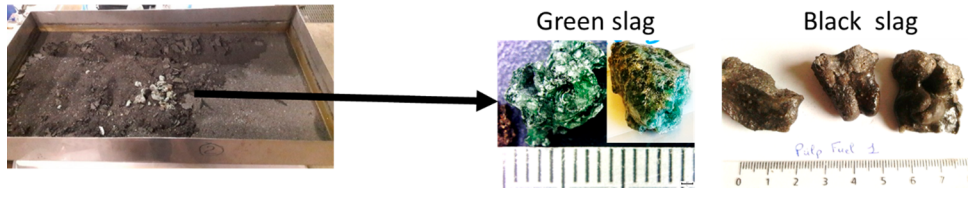

Figure 7. Residues collected after drying.

https://doi.org/10.1021/acs.energyfuels.1c00993
Energy Fuels 2021, 35, 12151−12164

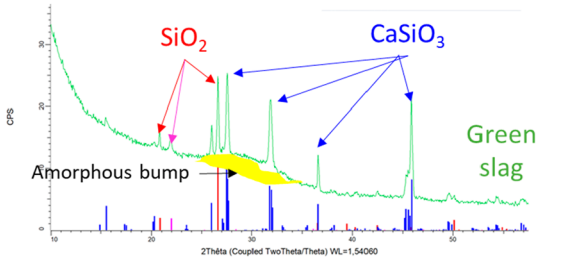

a- P-XRD diffractogram of the green slag

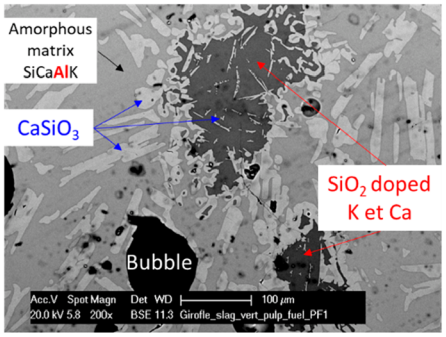

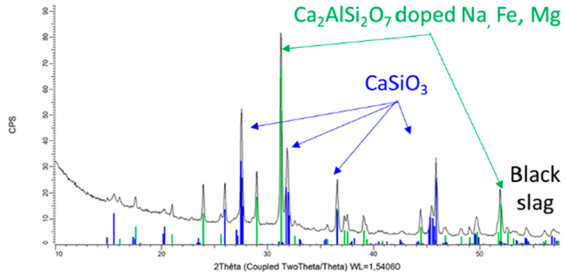

c- P-XRD of the black slag

EDS (Wt%)	O	Na	Mg	Al	Si	P	K	Ca	Ti	Fe
SEM-EDS SiO_2 doped	45	0.8	1	2	**34**		7.5	7.5		1
SEM-EDS Amorphous matrix	43	0.8	1.7	**6.5**	**22**	0.5	**3.5**	**19**	0.2	2
ICP Green slag		0.7	1.3	**6.2**	23	0.4	2.7	22		1.7
ICP HW bark ash		0.5	1.3	2.6	19	0.5	4.2	23	0.1	1.5

b- SEM-EDS analysis of the green slag

Figure 9. Characterization of black and green slags.

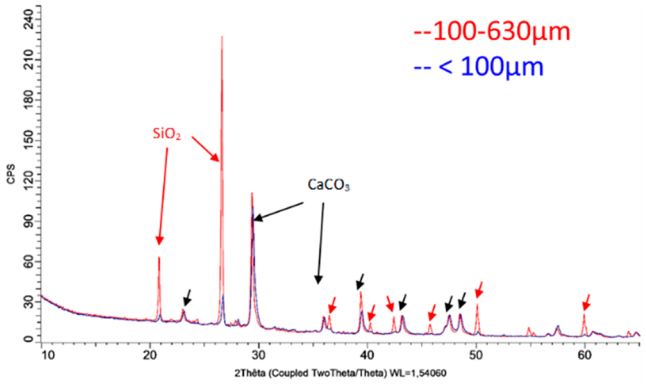

Figure 10. P-XRD on residues of <100 μm (blue) and 100−630 μm (red).

coming during the biomass injection are supposed to be dissolved in the full water present at the bottom of the reactor at the same time as water is overflowing.

The main cations are Ca^+ and K^+, and the main anion is NO_3^-. The pH is acidic. Carbonate (CO_3^-) and hydrogenocarbonate (HCO_3^-) anions were not measured. They should be very low with mainly CO_2 (g) dissolved in water as a result of the very acidic pH.

To explain the acidic pH and such a large amount of NO_3^-, water was sampled just before the biomass injection and characterized in another test. An acidic pH and a very high concentration of NO_3^- were also evidenced, with almost no other ionic species. This indicates that the high temperature and oxidizing gas of the natural gas/O_2 burner produce NO_x from injected N_2. Indeed, even when the biomass has not yet been injected, N_2 is injected to cool the end of the biomass supply system, which is located right next to the burner (Figure 1). Note that CO_2 (g) is also able to acidify the water, particularly in the first part of the test during the heating of the reactor by the natural gas/O_2 burner [CO_2 (g) ~ 25 vol %].

The large amount of calcium dissolved in water can also be explained by the acidic water that favors calcium oxide dissolution.

3.3. Overall and Elemental Mass Balance of Ashes. An overall mass balance was established in Figure 11 for the ash by comparing, at the inlet, the theoretical mass of ash injected (1795 g) that is calculated with the total mass of dry biomass injected multiplied by its ash yield at 815 °C (black circle in Figure 11) and, at the outlet, the mass of ash recovered at the bottom of the reactor (sum of ash mass from the solid residue and water-soluble residue). The former (1237 g) is calculated using the dried collected residues for each sieved fraction multiplied by each ash yield at 815 °C. The latter (522 g) shown as a green bar in Figure 11 is calculated with the mass of water collected at the bottom of the EFR multiplied by the concentration in water (from IC analyses) and considering that the inorganic elements are in the carbonate form.

The overall mass balance is well-closed (98%). It is noteworthy that about 69% of the ash mass is recovered in the solid residues and the rest, i.e., 29%, is dissolved in the

Table 6. Anions, Cations, and pH Measured in Water Collected at the Bottom of the EFR

NH_4^+ (mg/L)	Ca^+ (mg/L)	Mg^+ (mg/L)	K^+ (mg/L)	Na^+ (mg/L)	Cl^- (mg/L)	NO_3^- (mg/L)	NO_2^- (mg/L)	SO_4^- (mg/L)	pH	water collected (L)
<0.02	310	37	64	12	4	3190	0.23	<1	2.4	500

https://doi.org/10.1021/acs.energyfuels.1c00993
Energy Fuels 2021, 35, 12151−12164

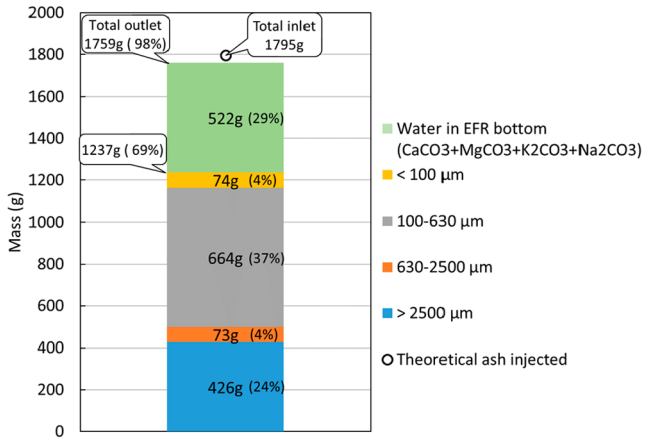

Figure 11. Overall mass balance of ashes.

water. The smallest particles (<100 μm) represent only 4%. This class probably contains the fly ash (<10 μm) because almost none is measured in the filter at the exhaust of the reactor.

An elemental mass balance of ashes was performed in the same way as the overall one for each inorganic element. All solid residues were analyzed by ICP, and the water was analyzed by IC (Figure 12).

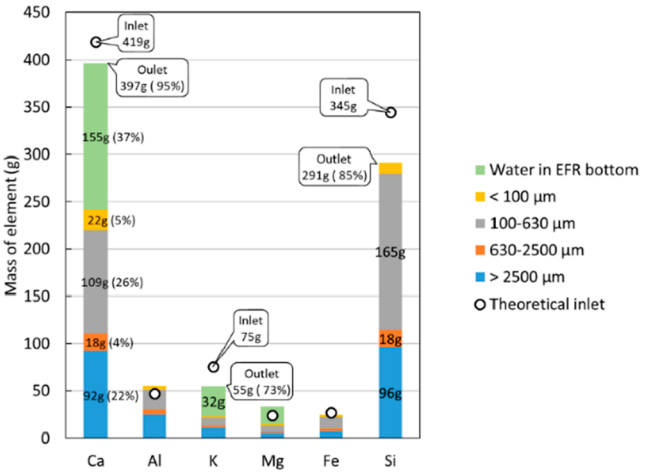

Figure 12. Elemental mass balance of ashes.

The elemental mass balance is only shown for the elements that were introduced into the reactor with a mass high enough (i.e., >10 g) to have a chance to be recovered in the reactor. Elements S, Cl, Na, and P are thus not shown. N is not shown either, even if its inlet mass is high (97 g), because there is almost 4 times more N measured in the water than introduced into the reactor as a result of N_2 oxidized to NO_x in the burner flame and then dissolved in the water (see section 3.2.4).

However, the mass balance is still performed anyway for S (inlet mass = 8.3 g) because H_2S and COS were clearly measured by μGC at the exhaust of the reactor, giving 72% recovered, which is not an odd result. S recovered in slags was 5% and less than 1% in the water. The total mass balance of S is thus calculated to be 77% S, which is not too bad.

For the two main elements (Ca and Si), the mass balance is almost closed (95 and 85%). Ca is the main element soluble in acidic water. Some Mg and K were also dissolved. The missing Si, Ca, and K elements in the mass balance are probably left in the slag sticking on the wall reactor.

The quite high amount of K soluble in the water (~44%) is not mainly coming from KCl nor K_2SO_4 because a very small amount of Cl^- and SO_4^- is recovered in the water. This is in agreement with quench effluent measurements during bark gasification in EFR.[12] It must be due to some KOH (g) and/or K (g) soluble in water as predicted by thermodynamic equilibrium calculations.[28]

The attempt to calculate Cl recovered in the water is 29% (2 g over 6.9 g at the inlet). Cl was not measured in the solid residues and not detected by P-XRD. No conclusion can be drawn.

Note that the Mg and Fe inlet amounts are too small (~20 g) to really conclude. It is not the case for Al introduced in a higher amount (~50 g at the inlet). A higher amount of Al was collected at the outlet than introduced with the feedstock, confirming the slight alumina pollution by the reactor wall.

3.4. Simulation Tools and Comparison to Experiments. *3.4.1. Thermodynamic Calculations Using a Phase Diagram.* The phase diagram of the three main oxides of HW bark ashes (SiO_2−CaO−K_2O) calculated at 1300 and 1400 °C is shown in Figure 13. The temperature of the tests is closer to 1300 °C rather than 1400 °C (Figure 2). The green-, white-, and red-colored areas correspond to 100% solid, solid + liquid, and 100% liquid, as explained in De Fusco and Defoort[29] to better understand these isothermal sections of the phase diagrams. The liquidus temperature is the boundary line between the liquid and solid + liquid area (boundary between white and red areas). When the temperature is increased from 1300 to 1400 °C, the liquid area is obviously increased.

The HW bark ash composition is plotted (pink triangle) in Figure 13 at 1300 and 1400 °C. It is predicted to be solid ($CaSiO_3$) + liquid even at 1400 °C. These results are in agreement with the phases observed by P-XRD for the black and green slags characterized previously.

3.4.2. Thermodynamic Calculations Using Global Calculations. The previous conclusions were obtained by analyzing only the three main oxides. A small content of other elements could change the phase behavior. Global calculations were conducted with all of the elements of HW bark and taking into account the atmosphere and total pressure. The assumptions and initial mass balance are reported in Tables S2−S4 of the Supporting Information.

Figure 14 shows the prediction of the effect of the temperature on the nature of the condensed phases (solid + liquid).

It is observed that the solidus temperature, i.e., apparition of the liquid phase (called SLAGA), is calculated at 1043 °C and the liquidus temperature, i.e., disappearance of any solid phase, is calculated at 1349 °C.

The main solid phase in equilibrium with the liquid phase is $CaSiO_3$ (wollastonite) in the whole range of temperatures. This is in agreement with the phase diagram approach with the three main oxides (Figure 13). These predictions are in agreement with the P-XRD results collected on the large particle size residues (>2500 μm, i.e., black and green slag).

Other phases in smaller quantity, such as Ca−Mg silicate ($Ca_3MgSi_2O_8$) and some K−Al silicates [$KAlSi_2O_6$ (leucite) and $KAlSiO_4$ (kalsilite)], are predicted to appear at lower temperatures. They are not observed by P-XRD probably because they are in too small amount or as a result of the solidification pathway. Instead, the crystalline phase SiO_2

https://doi.org/10.1021/acs.energyfuels.1c00993
Energy Fuels 2021, 35, 12151−12164

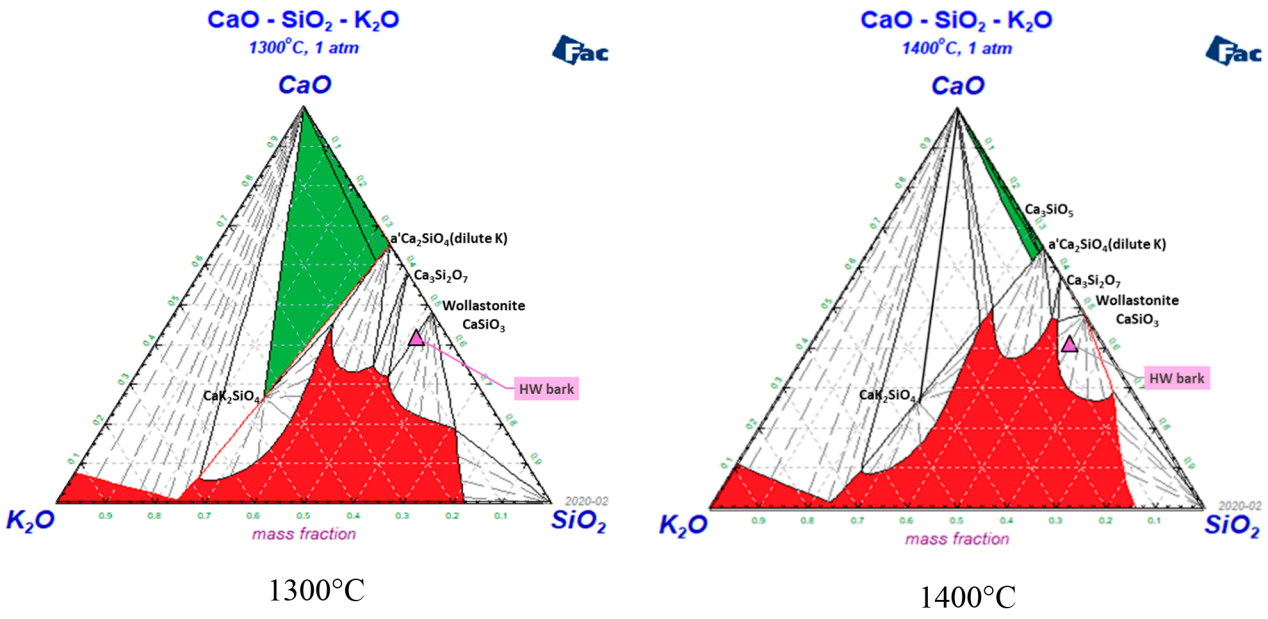

Figure 13. SiO_2−CaO−K_2O phase diagram calculated with FactSage 7.3 and the database FToxid7.3.

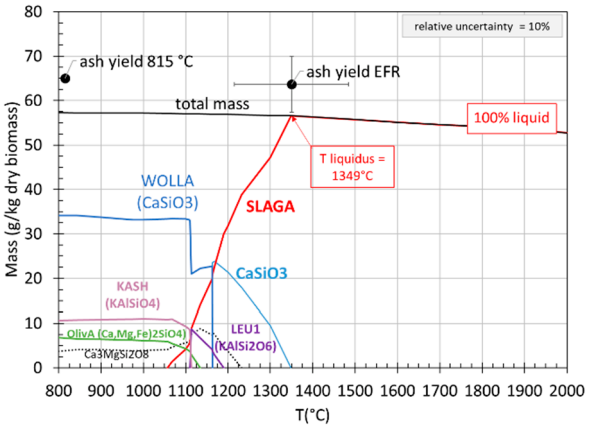

Figure 14. Mass of condensed phases predicted (g/kg of dry biomass) (lines) and measured ash yield at 815 °C and ash yield of the EFR test (black round dots). A typical relative uncertainty of 10% is shown.

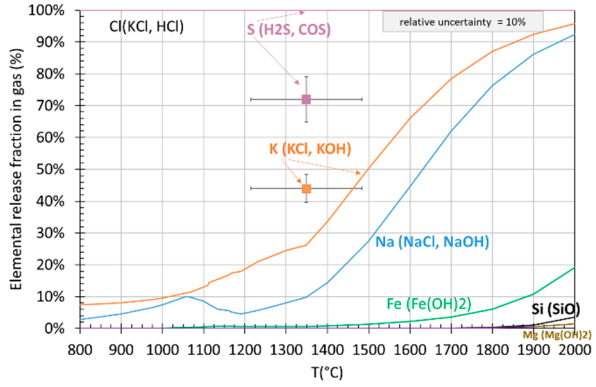

Figure 15. Elemental volatilization predicted (lines) and measured (square dots). A typical relative uncertainty of 10% is shown.

(quartz) is observed by P-XRD for the green slag along with doped $Ca_2AlSi_2O_7$ (melilite) for the black slag.

The smaller class of residues (<630 μm) is composed of SiO_2 and $CaCO_3$ that are not predicted.

The total mass of the condensed phase is calculated between 57 g at 800 °C and 53 g at 2000 °C close to the experimental ash yield measured at 815 °C in air and from the mass balance in the EFR (65 and 62 g/kg, db, respectively).

The volatilization of each element is calculated in Figure 15. The main gaseous species involved are shown in parentheses.

A full volatilization of S (as H_2S and COS) and Cl (as KCl and HCl) is calculated from 800 °C. A comparison to experimental results is uncertain because these elements are introduced into the reactor with a mass (i.e., 8.3 g of S and 6.9 g of Cl) too low to have a chance to be recovered in the reactor. However, some H_2S and COS are clearly measured by μGC, showing that 72% of S is in the gas phase, which is the good tendency predicted.

In the temperature range of the EFR test (1000−1400 °C), about 10−30% of initial K (as KCl and KOH) and about 10% of Na (as NaCl and NaOH) are predicted to be released in the gas phase. The measure of volatilized K is taken from K soluble in water after being released in the gas phase. The unknown mass of K in Figure 15 was taken into account by distributing it over all of the measurements (gases and solids). It is measured at 44%, which is a little higher than predicted.

The composition of the liquid phase (SLAGA) is plotted in weight percent versus the temperature in Figure 16a.

The liquid phase is predicted to be rich in SiO_2 and then CaO, Al_2O_3, and K_2O. When the temperature increases, CaO strongly increases as a result of the dissolution of the Ca-rich condensed phases, which cause the decrease of the other oxides by the dilution effect. Above the liquidus temperature of 1348 °C, K_2O is decreasing as a result of the K volatilization as KOH (g) and K (g). The measured composition of the green and black slags is shown by comparison in Figure 16b. The green slag composition measured is close to the 1200 °C calculated value, except that of K_2O, which is measured lower. This may be due to the volatility of K, which is measured

https://doi.org/10.1021/acs.energyfuels.1c00993
Energy Fuels 2021, 35, 12151−12164

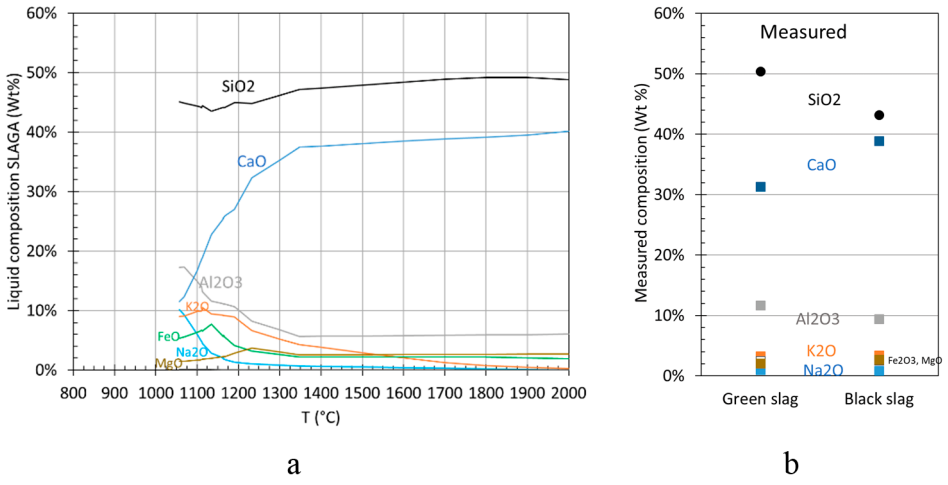

Figure 16. Composition of the liquid phase (a) predicted and (b) measured.

slightly higher than that calculated (Figure 15). The black slag does not fit with any temperature.

To explain the black slag composition and its Ca−Al silicate (melilite) observed by P-XRD, the effect of the interaction between the ashes and the ceramic refractory materials of the reactor wall, dense alumina in the upper part and refractory concrete (60% Al_2O_3−40% SiO_2) in the lower conical part, is also calculated at 1150 °C. The main calculated condensed phases are shown in Figure 17.

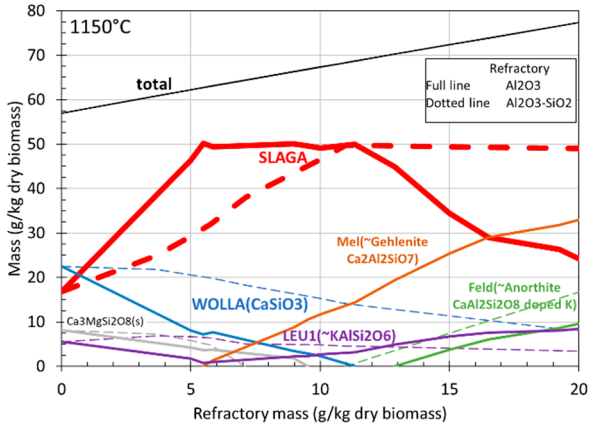

Figure 17. Mass of condensed phases when ashes are in an interaction with Al_2O_3 (full line) or Al_2O_3−SiO_2 (dotted line) predicted (g/kg of dry biomass).

Both refractories have fully reacted (i.e., no excess of Al_2O_3 nor Al_2O_3−SiO_2 remains at equilibrium) up to 20 g/kg, db, of the refractory. They first dissolved in the liquid-phase SLAGA, whose amount increased with the increased amount of refractory. The liquid phase increased faster for the dense alumina rather than with the refractory concrete and stabilized after reacting with 5.5 g of Al_2O_3 (11 g of Al_2O_3−SiO_2).

When the solubility limit is reached, a new solid phase rich in alumina appears (gehlenite $Ca_2Al_2SiO_7$ for Al_2O_3 and anorthite $CaAl_2SiO_8$ for Al_2O_3−SiO_2). Both phases are Ca−Al silicates as observed for the black slag by P-XRD.

The composition of the liquid phase (SLAGA) is reported in Figure 18.

The same composition is observed regardless of the refractory dissolution (slightly higher silica for the refractory Al_2O_3−SiO_2). When the mass of the refractory increases, the compositions in Al_2O_3 and CaO increase and those in K_2O and SiO_2 decrease.

When the calculated composition of the liquid phase (Figure 18a) is compared to the measured composition for the black slag (Figure 16b), a better agreement is observed within the alumina contents for both slags. However, a higher calcia content is measured.

3.4.3. Thermodynamic Calculations: Discussion. These results show good consistency between experimental results collected on the large particle size residues (>2500 μm, i.e., black and green slag) and the prediction either from a simple phase diagram or with global calculations. In this case, the effect of the other elements does not change the prediction of the main solid phases in equilibrium with the liquid.

Carlsson et al.[13] found that global calculations with FactSage 6.4 could not adequately reproduce measurements (slag composition and K volatilization), which is in contradiction with the good reproducibility that we observed with our experiments. The more recent database that we used is not the reason for this contradiction. In fact, the fuel by Carlsson et al. and ours are very different, even though they both come from woody biomass. The fuel by Carlsson et al. is a clean woody biomass whose composition is SiO_2-poor. On the contrary, we used a HW bark polluted by soil whose composition is in the SiO_2-rich part of the SiO_2−CaO−K_2O phase diagram (Figure 13). It is possible that our prediction is closer to the measurements because the SiO_2-rich part of the ternary phase diagram is best known.[30] Another explanation could be to take into account the interaction between the ashes and the refractory in the input of the global calculation by Carlsson et al. We performed this simulation using their inputs and found that the solidus temperature decreased strongly, K was trapped in the liquid slag, and its volatility decreased. These predictions are then closer to the experimental findings of Carlsson et al. Carlsson et al.[13] and Ma et al.[31] proposed a more complex scheme in several calculation steps, including the fractionation between the gas and the condensed phase of the ash. Our results show that it is not necessary to perform such refined calculations to reproduce the experimental results.

The effect of a silica-rich biomass or a woody biomass polluted by silica was already pointed out by Ma et al.[11,12] to favor the melt formation and its strong interaction with the

https://doi.org/10.1021/acs.energyfuels.1c00993
Energy Fuels 2021, 35, 12151−12164

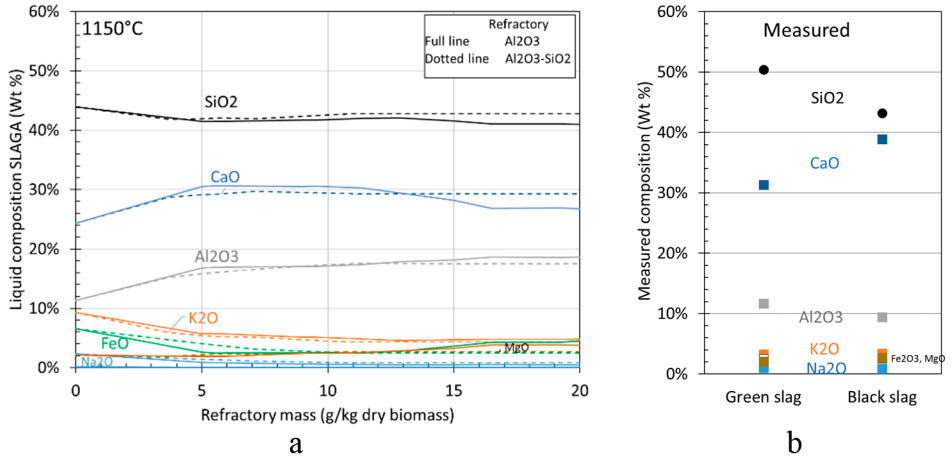

Figure 18. Composition of the liquid phase (a) predicted when ashes are in an interaction with Al_2O_3 (full line) or Al_2O_3−SiO_2 (dotted line) and (b) measured (same figure as Figure 16b).

refractory wall. Our experimental results do not show such a strong interaction of the ash with the refractory material.

However, it is noteworthy that the good consistency between experimental and predicted results was obtained for the larger particle size residues (>2500 μm, i.e., black and green slag) corresponding to only 24 wt % (Figure 11) of the collected residues instead of 100 wt % of the total ash mass, as predicted in Figure 14. The rest of the ashes, i.e., about 70 wt %, consisting of the smaller class of residues (<630 μm) and the ash dissolved in the water quench, is composed of SiO_2 and $CaCO_3$, which was not predicted by calculations. This shows that a large amount of the ash (~70 wt %) does not seem to be in thermodynamic equilibrium. It seems that a part of the soil (SiO_2) and the compounds (CaO, $CaCO_3$, CaC_2O_4, KCl, etc.) initially present in the raw HW bark[3,27] did not react together to give $CaSiO_3$ and the liquid phase.

Then, it seems that one global calculation is sufficient to obtain reliable results for the slag composition and K volatilization. This global calculation takes into account the ash fractionation and the chemical reaction between the refractory wall and the gas and ashes. However, it is possible that only a part of the silica from soil reacted with the other native elemental form of the woody biomass or with the refractory as a result of kinetic or hydrodynamic reasons.

3.4.4. Viscosity Calculations. Prediction of the viscosity of the ashes is shown in Figure 19 from the composition of the liquid phase calculated at equilibrium with FactSage (red line) and from measurements of the composition of the black (black line) and green (green line) slags. For the slag to flow along the reactor wall, it is generally accepted that the slag viscosity must be sufficiently low at the temperature of tapping, typically less than 10−25 Pa s (arrow represented in Figure 19).[32]

Above the predicted liquidus temperature (>1348 °C), the viscosity calculated from the calculated liquid composition or from the measured black and green slag compositions is less than 10 Pa s.

Below the liquidus temperature as a result of the solid fraction increasing, the viscosity is sharply increasing and reaches a viscosity higher than 25 Pa s for a temperature below ~1200 °C (model prediction by Thomas).

The maximum temperature measured at the level of the cone (T14−T16 of 1.15 m; Figure 2) is around 1000 and 1200 °C at the level above (T18 of 0.935 m; Figure 2). Both

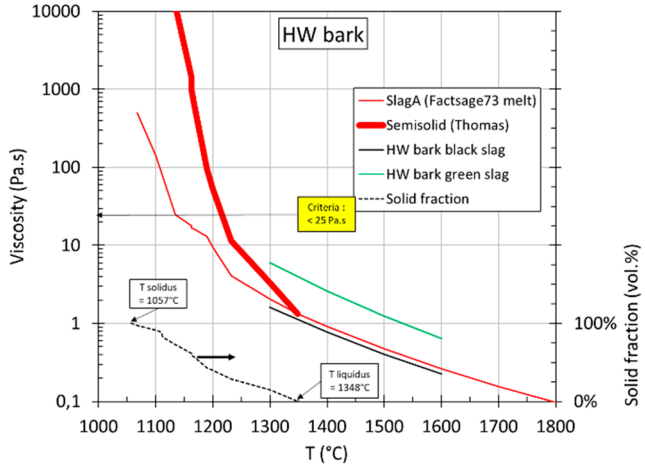

Figure 19. Viscosity calculations of the HW bark ashes (lines) and volumetric solid fraction calculated with FactSage (dotted line).

slags collected (black or green) looked glassy like solidified silicate liquid (Figure 7) even if the black slag seemed to be more crystallized by P-XRD because of a slower solidification. When all of the uncertainties in the viscosity calculations and in the temperature gradient are taken into account, these calculations are in qualitative agreement with the fact that the slags collected probably flowed along the bottom of the reactor wall.

These viscosity calculations do not agree with the results found by Ma et al.[12,13] regarding their bark wood and their wood. Their viscosities were much higher (>10^4 Pa s) for temperatures less than 1350 °C. As already pointed out, the main reason is the composition of the HW bark of our study, which is much richer in silica (as a result of soil pollution) than their bark wood.[12] The solidus/liquidus temperatures of the HW bark are thus lower (~100 °C) than those of their bark wood (1057/1348 versus 1140/1480 °C). The influence of the solid fraction strongly increases the viscosity in the working EFR temperature range (1250−1350 °C) of their bark wood. The viscosity is known to be higher for SiO_2-rich liquid. Nevertheless, the effect of the solid fraction in a SiO_2-poor liquid is also very effective in increasing the viscosity.

https://doi.org/10.1021/acs.energyfuels.1c00993
Energy Fuels 2021, 35, 12151−12164

4. CONCLUSION

HW bark was gasified on a pilot scale in a pressurized slagging EFR (250 kW_{th}) in allothermal conditions, with a 6 kg/h feeding rate during 5 h, a total pressure of 5 bar, and a maximum wall temperature of 1300−1350 °C. Consistent results were obtained for the gas composition. No blockage linked to the ash/slag was observed, even though about 1.8 kg of the theoretical ash mass was injected. More than 95% of carbon from the biomass was converted into gas species.

About 1.9 kg of dried residue was collected at the bottom of the reactor, corresponding to 1.3 kg of ash and 0.6 kg of unburned carbon. A high amount of ash was dissolved in the water quench mainly as Ca and K cations. A high amount of NO_3^- anions was also measured in the water quench coming from the oxidation of the introduced N_2 gas (and not from the N biomass) in the high-temperature zone of the O_2/CH_4 burner and was mainly responsible for the acidic pH. The overall ash and (Ca, K, and Si) mass balances were both well-closed.

Predictive calculation at equilibrium of the main condensed phases, i.e., $CaSiO_3$ and liquid (amorphous), were in agreement with the P-XRD observations for only $^1/_4$ of the collected ashes. The remaining ashes ($^3/_4$) were composed of phases that were not predicted by calculations: SiO_2 probably from soil and $CaCO_3$ from compounds initially present in the raw HW bark. This shows that only a part of the polluted soil reacted with the raw HW bark ash. Slight pollution by the alumina wall of the reactor was observed and confirmed by calculations. A very small amount (<4%) of fly ashes was noticed.

Viscosity calculations are below the criteria of 25 Pa s in the temperature range of the test.

■ ASSOCIATED CONTENT

Supporting Information

The Supporting Information is available free of charge at https://pubs.acs.org/doi/10.1021/acs.energyfuels.1c00993.

List of solutions taken into account for the thermodynamic calculations with the FactSage software (Table S1) as well as the initial mass balance to perform the calculations (Tables S2−S4), example of FactSage results (section 3), and some EDX semi-quantifications of residues collected on the top and bottom of the EFR windows (Table S5) (PDF)

■ AUTHOR INFORMATION

Corresponding Author

Françoise Defoort − *Université Grenoble Alpes (UGA), Commissariat à l'Energie Atomique et aux Energies Alternatives (CEA), Laboratoire d'Innovation pour les Technologies des Energies nouvelles et les Nanomatériaux (LITEN), Département Thermique Conversion et Hydrogène (DTCH), Laboratoire Réacteur et Procédés (LRP), F-38000 Grenoble, France*; orcid.org/0000-0001-8805-4705; Email: francoise.defoort@cea.fr

Authors

Boris Grangier − *Université Grenoble Alpes (UGA), Commissariat à l'Energie Atomique et aux Energies Alternatives (CEA), Laboratoire d'Innovation pour les Technologies des Energies nouvelles et les Nanomatériaux (LITEN), Département Thermique Conversion et Hydrogène (DTCH), Laboratoire Réacteur et Procédés (LRP), F-38000 Grenoble, France*

Thierry Chataing − *Université Grenoble Alpes (UGA), Commissariat à l'Energie Atomique et aux Energies Alternatives (CEA), Laboratoire d'Innovation pour les Technologies des Energies nouvelles et les Nanomatériaux (LITEN), Département Thermique Conversion et Hydrogène (DTCH), Laboratoire Réacteur et Procédés (LRP), F-38000 Grenoble, France*

Serge Ravel − *Université Grenoble Alpes (UGA), Commissariat à l'Energie Atomique et aux Energies Alternatives (CEA), Laboratoire d'Innovation pour les Technologies des Energies nouvelles et les Nanomatériaux (LITEN), Département Thermique Conversion et Hydrogène (DTCH), Laboratoire Réacteur et Procédés (LRP), F-38000 Grenoble, France*

Gilles Ratel − *Université Grenoble Alpes (UGA), Commissariat à l'Energie Atomique et aux Energies Alternatives (CEA), Laboratoire d'Innovation pour les Technologies des Energies nouvelles et les Nanomatériaux (LITEN), Département Thermique Conversion et Hydrogène (DTCH), Laboratoire Réacteur et Procédés (LRP), F-38000 Grenoble, France*

Sylvie Valin − *Université Grenoble Alpes (UGA), Commissariat à l'Energie Atomique et aux Energies Alternatives (CEA), Laboratoire d'Innovation pour les Technologies des Energies nouvelles et les Nanomatériaux (LITEN), Département Thermique Conversion et Hydrogène (DTCH), Laboratoire Réacteur et Procédés (LRP), F-38000 Grenoble, France*

Complete contact information is available at: https://pubs.acs.org/10.1021/acs.energyfuels.1c00993

Notes

The authors declare no competing financial interest.

■ ACKNOWLEDGMENTS

This work has received funding from the European Union's Horizon H2020 Research and Innovation Program under Grant Agreement 818011. The French Agency for Research (ANR) is also acknowledged for having partly funded the GIROFLE EFR within the framework of EQUIPEX 2011 Equipment of Excellence of the Future Investments Program.

■ REFERENCES

(1) Wang, P.; Massoudi, M. Slag Behavior in Gasifiers. Part I: Influence of Coal Properties and Gasification Conditions. *Energies* **2013**, *6* (2), 784−806.

(2) Van der Drift, A.; Boerrigter, H.; Coda, B.; Cieplik, M. K.; Hemmes, K. *Entrained Flow Gasification of Biomass. Ash Behaviour, Feeding Issues, System Analyses*; Energy Research Centre of the Netherlands (ECN): Petten, Netherlands, 2004; Technical Report ECN-C-04-039.

(3) Vassilev, S. V.; Baxter, D.; Andersen, L. K.; Vassileva, C. G. An Overview of the Chemical Composition of Biomass. *Fuel* **2010**, *89*, 913−933.

(4) Coda, B.; Cieplik, M. K.; de Wild, P. J.; Kiel, J. H. A. Slagging Behavior of Wood Ash under Entrained-Flow Gasification Conditions. *Energy Fuels* **2007**, *21*, 3644−3652.

(5) Leiser, S.; Cieplik, M. K.; Smit, R. Slagging Behavior of Straw and Corn Stover and the Fate of Potassium under Entrained-Flow Gasification Conditions. *Energy Fuels* **2013**, *27* (1), 318−326.

(6) Qin, K.; Lin, W.; Fæster, S.; Jensen, P. A.; Wu, H.; Jensen, A. D. Characterization of Residual Particulates from Biomass Entrained Flow Gasification. *Energy Fuels* **2013**, *27* (1), 262−270.
(7) Bläsing, M.; Müller, M. Release of Alkali Metal, Sulfur, and Chlorine Species during High-Temperature Gasification of Coal and Coal Blends in a Drop Tube Reactor. *Energy Fuels* **2012**, *26*, 6311−6315.
(8) De Fusco, L.; Blondeau, J.; Defoort, F.; Jeanmart, H.; Contino, F. Characterization of Sunflower Husks Fouling in a Drop Tube Furnace: Comparison of Deposits with H_3PO_4, $CaCO_3$ and $Al_2Si_2O_5(OH)_4$ Additives. *Proceedings of the 24th European Biomass Conference and Exhibition*; Amsterdam, Netherlands, June 6−9, 2016; pp 748−755, DOI: 10.13140/RG.2.2.17818.44481.
(9) Wagner, D. R.; Holmgren, P.; Skoglund, N.; Broström, M. Design and Validation of an Advanced Entrained Flow Reactor System for Studies of Rapid Solid Biomass Fuel Particle Conversion and Ash Formation Reactions. *Rev. Sci. Instrum.* **2018**, *89* (6), 065101.
(10) Holmgren, P.; Broström, M.; Backman, R. Slag Formation during Entrained Flow Gasification: Silicon-Rich Grass Fuel with a $KHCO_3$ Additive. *Energy Fuels* **2018**, *32* (10), 10720−10726.
(11) Ma, C.; Weiland, F.; Hedman, H.; Boström, D.; Backman, R.; Öhman, M. Characterization of Reactor Ash Deposits from Pilot-Scale Pressurized Entrained-Flow Gasification of Woody Biomass. *Energy Fuels* **2013**, *27*, 6801−6814.
(12) Ma, C.; Carlborg, M.; Hedman, H.; Wennebro, J.; Weiland, F.; Wiinikka, H.; Backman, R.; Ohman, M. Ash Formation in Pilot-Scale Pressurized Entrained-Flow Gasification of Bark and a Bark/Peat Mixture. *Energy Fuels* **2016**, *30*, 10543−10554.
(13) Carlsson, P.; Ma, C.; Molinder, R.; Weiland, F.; Wiinikka, H.; Öhman, M.; Öhrman, O. Slag Formation during Oxygen-Blown Entrained-Flow Gasification of Stem Wood. *Energy Fuels* **2014**, *28* (11), 6941−6952.
(14) Seebold, S.; Eberhard, M.; Wu, G.; Yazhenskikh, E.; Sergeev, D.; Kolb, T.; Muller, M. Thermophysical and Chemical Properties of Bioliq Slags. *Fuel* **2017**, *197*, 596−604.
(15) Cavagnol, S. M.; Covella, K.; Müller-Hagedorn, M. Determination of Slag Deposition Rate on Cooling Screen Reactor Walls by Utilisation of Slag Thickness Measurements. *Fuel* **2018**, *228*, 369−378.
(16) Dahmen, N.; Abeln, J.; Eberhard, M.; Kolb, T.; Leibold, H.; Sauer, J.; Stapf, D.; Zimmerlin, B. The Bioliq Process for Producing Synthetic Transportation Fuels. *Wiley Interdiscip. Rev.: Energy Environ.* **2017**, *6* (3), 1−10.
(17) Jung, I.-H.; Van Ende, M.-A. Computational Thermodynamic Calculations: FactSage from CALPHAD Thermodynamic Database to Virtual Process Simulation. *Metall. Mater. Trans. B* **2020**, *51* (5), 1851−1874.
(18) Seiler, J.-M. CEA Research Activities in the Field of Entrained Flow Reactors. *Proceedings of the 2nd International Freiberg Conference on IGCC & XtL Technologies*; Freiberg, Germany, May 8−12, 2007.
(19) Urbain, G. Viscosity Estimation of Slags. *Steel Res.* **1987**, *58*, 111−116.
(20) Bale, C. W.; Belisle, E.; Chartrand, P.; Decterov, S. A.; Eriksson, G.; Hack, K.; Jung, I. H.; Kang, Y. B.; Melancon, J.; Pelton, A. D.; Robelin, C.; Petersen, S. FactSage Thermochemical Software and Databases—Recent Developments. *CALPHAD: Comput. Coupling Phase Diagrams Thermochem.* **2009**, *33*, 295−311.
(21) Duchesne, M. A.; Bronsch, A. M.; Hughes, R. W.; Masset, P. J. Slag Viscosity Modeling Toolbox. *Fuel* **2013**, *114*, 38−43.
(22) Wu, G.; Seebold, S.; Yazhenskikh, E.; Tanner, J.; Hack, K.; Müller, M. Slag Mobility in Entrained Flow Gasifiers Optimized Using a New Reliable Viscosity Model of Iron Oxide-Containing Multicomponent Melts. *Appl. Energy* **2019**, *236*, 837−849.
(23) Thomas, D. G. Transport Characteristics of Suspension.8. a Note on Viscosity of Newtonian Suspensions of Uniform Spherical Particles. *J. Colloid Sci.* **1965**, *20*, 267.
(24) Kondratiev, A.; Ilyushechkin, A. Flow Behaviour of Crystallising Coal Ash Slags: Shear Viscosity, Non-Newtonian Flow and Temperature of Critical Viscosity. *Fuel* **2018**, *224*, 783−800.
(25) Mills, K. C.; Rhine, J. M. The Measurement and Estimation of the Physical Properties of Slags Formed during Coal Gasification: 1. Properties Relevant to Fluid Flow. *Fuel* **1989**, *68* (2), 193−200.
(26) Lange, R. A. A Revised Model for the Density and Thermal Expansivity of K_2O−Na_2O−CaO−MgO−Al_2O_3−SiO_2 Liquids from 700 to 1900 K: Extension to Crustal Magmatic Temperatures. *Contrib. Mineral. Petrol.* **1997**, *130* (1), 1−11.
(27) Werkelin, J.; Skrifvars, B.-J.; Zevenhoven, M.; Holmbom, B.; Hupa, M. Chemical Forms of Ash-Forming Elements in Woody Biomass Fuels. *Fuel* **2010**, *89* (2), 481−493.
(28) Froment, K.; Defoort, F.; Bertrand, C.; Seiler, J. M.; Berjonneau, J.; Poirier, J. Thermodynamic Equilibrium Calculations of the Volatilization and Condensation of Inorganics during Wood Gasification. *Fuel* **2013**, *107*, 269−281.
(29) De Fusco, L.; Defoort, F. A Thermochemical Approach Based on Phase Diagrams to Characterize Biomass Ash and Select the Optimal Thermal Conversion Technology. *Proceedings of the 6th International Symposium on Energy from Biomass and Waste*; Venice, Italy, Nov 13−17, 2016.
(30) Morey, G.; Kracek, F. C.; Bowen, N. L. The Ternary System K_2O−CaO−SiO_2. *J. Soc. Glass Technol.* **1930**, *14* (54), 149−187.
(31) Ma, C.; Backman, R.; Ohman, M. Thermochemical Equilibrium Study of Slag Formation during Pressurized Entrained-Flow Gasification of Woody Biomass. *Energy Fuels* **2015**, *29*, 4399−4406.
(32) Hoy, H.; Roberts, A.; Wilkins, D. Behaviour of Mineral Matter in Slagging Gasification Process. *J. Inst. Gas Eng.* **1965**, *5*, 444−469.

https://doi.org/10.1021/acs.energyfuels.1c00993
Energy Fuels 2021, 35, 12151−12164